Multivalent recognition of histone tails by the PHD-fingers of CHD5

Samuel S. Oliver[1], **Catherine A. Musselman**[2], **Rajini Srinivasan**[3], **John P. Svaren**[3], **Tatiana G. Kutateladze**[2], and **John M. Denu**[1]

[1]Department of Biomolecular Chemistry, University of Wisconsin, Madison, WI 53706, USA

[2]Department of Pharmacology, University of Colorado Denver School of Medicine, Aurora, CO 80045 USA

[3]Department of Comparative Biosciences, Waisman Center, University of Wisconsin–Madison, Madison, Wisconsin 53705

Abstract

The chromodomain, helicase, DNA-binding protein 5 (CHD5) is a chromatin remodeling enzyme which is implicated in tumor suppression. In this study, we demonstrate the ability of the CHD5 PHD-fingers to specifically recognize the unmodified N-terminus of histone H3. We use two distinct modified peptide-library platforms (beads and glass slides) to determine the detailed histone binding preferences of PHD_1 and PHD_2 alone, and the tandem PHD_{1-2} construct. Both domains displayed similar binding preferences for histone H3, where modification (e.g. methylation, acetylation, and phosphorylation) at H3R2, H3K4, H3T3, H3T6 and H3S10 disrupts high-affinity binding, and the three most N-terminal amino acids (ART) are crucial for binding. The tandem $CHD5-PHD_{1-2}$ displayed similar preferences to those displayed by each PHD finger alone. Using NMR, surface plasmon resonance, and two novel biochemical assays, we demonstrate that $CHD5-PHD_{1-2}$ simultaneously engages two H3 N-termini and results in a 4-11 fold increase in affinity compared with either PHD-finger alone. These studies provide biochemical evidence for the utility of tandem PHD-fingers to recruit protein complexes at targeted genomic loci, and provide the framework for understanding how multiple chromatin-binding modules function to interpret the combinatorial PTM capacity written in chromatin.

Introduction

The chromodomain, helicase, DNA-binding (CHD) protein family falls into a class of enzymes that use energy derived from ATP hydrolysis to alter histone-DNA contacts within chromatin (1). There are nine members of the CHD family of proteins (CHD1-9) characterized by two signature motifs: tandem chromodomains near the N-terminus and an SNF2-like ATPase domain located in the central region of the protein sequence (1) (Figure 1a)

Of the known CHD family members, CHD4 (also known as Mi-2β) is the best characterized. It has broad tissue distribution and exists in the Mi-2/nucleosome remodeling and deacetylase (NuRD) complex, which couples histone deacetylation and chromatin remodeling ATPase activities. A decade of research has uncovered a number of connections

between the Mi-2/NuRD complex and a myriad of cellular processes including gene regulation, cell cycle progression, stem cell biology and oncogenesis (2-11).

A number of PHD fingers, including those of AIRE, BHC80, CHD4 and DNMT3L can recognize unmodified histone H3 (30). Structural analysis reveals that these PHD fingers bind the first several residues of the histone H3 tail in an extended binding pocket, stabilizing the complex through a network of hydrogen bonds and salt bridges. The residues important for histone tail interaction in the homologous CHD4 PHD1 and PHD2 fingers are conserved in CHD5.

Though CHD5 shares a high degree of sequence similarity with CHD4, (Figure 1) its expression is predominantly brain specific (12, 13). Interestingly, CHD5 mutation, deletion and down regulation is implicated in a multitude of different cancer types such as neuroblastoma, glioma, melanoma, prostate, ovarian, gastric, lung, and laryngeal (14-25). There is some evidence of aberrant CHD5 promoter methylation as the cause of down regulation in certain cancer types. One study, which analyzed the DNA methylation profiles for all nine CHD family members, found that CpG island hypermethylation was unique to only the CHD5 promoter in human cancer cell lines and primary tumors, particularly gliomas, colon and breast carcinomas (18). RT-qPCR analyses were used to correlate CHD5 loss of expression with promoter hypermethylation. CHD5 mRNA levels were restored upon treatment with a DNA demethylating agent (18).

Most notable is the role of CHD5 in neuroblastoma tumor suppression (13, 26). The possibility of a single genetic deletion in neuroblastomas driving tumorigenesis led to the identification of CHD5 as a key tumor suppressor controlling proliferation, apoptosis, and senescence via the p19^{Arf}/p53 pathway (27-29). Early investigation of a panel of neuroblastoma cell lines found consistently low or undetectable expression levels of CHD5. This bolstered a potential tumor suppressive role for CHD5 (12, 28). Immunohistochemical analysis of 90 primary neuroblastic tumors demonstrated a strong association of CHD5 expression with favorable prognostic value (26). Interestingly, recent studies of prostate cancer have reported mutations in CHD5 (55) (24).

Recent work has revealed the ability of CHD5 to associate with a NuRD-like complex in mouse brain. Depletion of CHD5 with shRNA lead to altered expression of genes implicated in aging, Alzheimer's', and normal neuronal function (13). Chromatin immunoprecipitation (ChIP) experiments in cultured rat neurons found that signal for CHD5 was 2 to 10-fold higher than a control IP (IgG) at some target genes. Increased signal suggested the possibility of direct regulation by CHD5 (13). Though CHD5 is proposed to function as a chromatin remodeling protein, there is currently limited evidence to suggest it directly binds and modulates its target genes. Assessing the protein motifs of CHD5 and elucidating the biochemical properties required for association and regulation of target genes could provide a foundation for design strategies that modulate CHD5's tumor suppressive function (29).

Unique to members CHD3-5 are two N-terminal PHD-finger domains (12) (Figure 1a). The PHD-finger is a small modular protein domain of 50-80 amino acid residues that appears in a multitude of chromatin-associated proteins (30-32). The unifying characteristic of the PHD-finger family is an evolutionarily conserved Cys4-His-Cys3 motif, which serves to anchor two zinc atoms in a cross-brace topology (33-35). The PHD fold consists of a two-strand anti-parallel β-sheet and a C-terminal α-helix (not necessarily present in all PHD-fingers) (30, 32, 36-38). PHD-fingers are found in over 100 human proteins and besides the canonical zinc coordinating Cys4-His-Cys3 motif, their sequences vary widely. Many PHD-finger domains have the capability of recognizing methylated, unmethylated and, most recently, acetylated lysine residues on histone proteins (34, 35, 38-44).

Because CHD3-5 contain tandem PHD-finger domains (Figure 1) there is the possibility for each individual domain to recognize a specific histone modification, and the dual domains can display a combinatorial effect that is reflected in cooperative binding during readout of histone modification patterns (40, 44, 45)}. There are three similar, but subtly distinct, possibilities for combinatorial recognition by paired histone binding modules: 1) a tandem domain can cooperate to bind a single modification 2) a tandem domain can cooperate to bind two modifications on the same histone tail (same protein) or 3) paired domains can cooperate to bind two modifications on different histone tails (different proteins).

In this study, we utilized two different peptide-library platforms and multiple biochemical binding assays to demonstrate the ability of the CHD5 PHD-fingers to specifically recognize the unmodified N-terminus of histone H3. The binding selectivity for the tandem PHD-finger domain of CHD5 (CHD5-PHD$_{1-2}$) displayed minimal deviation from the preferences of each PHD-finger alone. The tandem PHD fingers of CHD5 simultaneously binds two H3 tails, leading to a significantly slower off rate on immobilized histone peptides. This avidity effect provides biochemical evidence for the ability of tandem chromatin reader domains to enrich chromatin complexes at target genomic loci.

Experimental Procedures

General methods

Amino acids were purchased from Novabiochem and Bachem. Tentagel resin was purchased from Peptides International. Microscope slides were purchased from Intavis Bioanalytical Instruments. All other chemicals and biochemicals were obtained from Sigma-Aldrich. The plasmid for GST fusion of the BHC80 PHD-finger (486-543) was obtained by Prof. Yang Shi. The PHD domains of CHD5 (PHD$_1$: 338-393; PHD$_2$: 413-468; PHD$_{1-2}$: 338-468) were fused with Glutathione-S-transferase in the pGEX-KG vector. Fusion proteins were purified as described. Solid phase and celluspot peptide synthesis was performed on an Intavis ResPep SL. Analytical gradient HPLC was performed on a Shimadzu series 2010C HPLC with a Vydac C18 column (10 Mm, 4.6×250 mm) and peptide purification performed on a Beckman BioSys 510 with a C18 column. Arraying was accomplished on a GeneMachines OmniGrid Arrayer with TeleChem SMP3 quill-like pins. Isothermal titration calorimetry was performed on a MicroCal VP-ITC Micro Calorimeter.

Celluspot library construction

Celluspot peptides were synthesized on acid soluble Fmoc-β-alanine etherified cellulose paper discs (1.0 μmol/cm^2 loading capacity) available from Intavis Bioanalytical Instruments. Standard amino acid building blocks were purchased from Peptides International. All modified amino acids are commercially available from Novabiochem and peptide reagents were obtained from Sigma Aldrich. Standard Fmoc mediated peptide synthesis was used and coupling was mediated by Cl-6-HOBt/HBTU/DIEA activation (5:5:8 equivalents). Peptide deprotection was performed using 150 uL of a side chain deprotection solution (trifluoroacetic acid/triisopropylsilane/water/dichloromethane: 80%, 3%, 5%, 12%) for 2 hrs at room temperature. Cellulose-peptide conjugates were solubilized overnight in 250 uL cellulose solvation solution (trifluoroacetic acid/trifluoromethansulfonic acid/triisopropylsilane/water: 88.5%, 4%, 2.5%, 5%). Ice-cold ether (750 uL) was added to the dissolved cellulose-peptide conjugate. The solution was briefly mixed and allowed to cool at 20 °C for 1 hr to facilitate precipitation. Precipitated conjugate was pelleted by centrifugation at 3000 rpm. The pellet was washed twice with fresh cold ether. After the final washing step residual ether was evaporated in a fume hood and 500 uL of dimethyl sulfoxide (DMSO) was added to the dried pellet in order to facilitate resolvation. The cellulose-peptide conjugate stock solutions were stored at 20 °C. Stock peptide solutions (6

uL) were transferred to a Genetix high sample recovery 384-well plate and 1 uL of $7\times$ SSC buffer (1 M NaCl; 100 µM $Na_3C_6H_5O_7$[circle4]$2H_2O$; pH 7.0) was added. The library was arrayed with the GeneMachines OmniGrid Arrayer with TeleChem SMP3 quill-like pins. A 0 ms dip time and 250 ms print time was used. Each member of the library was arrayed in a 4×4 grid with 500×500 µm spacing. Three libraries were arrayed on a single microscope slide (Intavis) and stored at $4°$ C until use. For construction of the H3unmod dilution library a peptide corresponding to the first eleven amino acids of histone H3 was synthesized in the same manner as described above and diluted using a blank celluspot disc dissolved in DMSO over two orders of magnitude.

H3 combinatorial library synthesis and on-bead assay

Details of the H3 library design and synthesis can be found in (46)

GST-based slide assay

Assays were performed using three-chambered SecureSeal™ hybridization gaskets (Grace Bio-Labs). After securing the gasket to the surface of the slide ~300 uL of TBST (50 mM Tris; 150 mM NaCl; 0.05% Tween-20; pH 7.5) was used to hydrate the chamber. The slide surface was subsequently blocked with a 1% BSA/TBST solution for 1 hr at room temperature. The blocking solution was aspirated and 300 µL of 1 µM (PHD_1 and PHD_2) or 100 nM (PHD_{1-2}) GST-PHD-finger in 1% BSA/TBST buffer was added for 1 hr at room temperature. The protein solution was aspirated and the chambers were washed three times with ~300 µL of TBST. A 1:2000 dilution of biotinylated GST antibody (Santa Cruz Biotechnology) in 1 % BSA/TBST buffer was added to the chamber and incubated for 1 hr at room temperature. The antibody solution was removed and the chambers were washed three times with ~300 µL of TBST. A 1:2000 dilution of streptavidin conjugated Alexa Fluor-647 (Invitrogen) in 1 % BSA/TBST buffer was added to the chamber and incubated for 1 hr at room temperature. The solution was aspirated and chamber washed three times with ~300 µL of TBST. The gasket was removed from the slide surface and the surface was rinsed briefly with water before being quickly dried under a stream of air. The fluorescent signal was detected on a Typhoon FLA 9000 and quantified using ImageQuant TL software (GE Healthcare)

Amplified Luminescent Proximity Homogeneous Assay (ALPHA)

Recombinantly purified CHD5-PHD finger proteins were diluted into StabilCoat buffer (Surmodics) at 100 µM concentration. Peptides corresponding to the first 11 amino acids from the histone H3 N-terminus were synthesized with either a $6\times$ His-repeat or biotin functionality. Stock solutions of peptide were made in StabilCoat buffer (1 µM). Proteins and peptide corresponding to each experimental condition were then diluted into a volume of 27 µL in ½ Area white 96-well plate (Perkin-Elmer) to yield a final concentration of 10 µM protein and 1 µM peptide. The plate was sealed and allowed to shake for 30 minutes at 200-300 rpm at ambient temperature. A small volume (3 µL) of 150 µg/mL donor and acceptor bead stock solution was added to each well for a working concentration of 15 µg/mL each bead. The solutions were allowed to shake for 30 minutes at 200-300 rpm at ambient temperature in the dark. Fluorescent emission was detected at 570/100 nm using a Biotek Synergy H4 plate reader and ALPHA specific filters.

^{15}N-Labeled Protein purification and NMR titrations

The CHD5 PHD_1, PHD_2 or PHD_{1-2} fingers were expressed in *E. coli* BL21(DE3) pLysS cells grown in $^{15}NH_4Cl$ supplemented minimal media. Bacteria were harvested by centrifugation after induction with IPTG (0.5 mM) and lysed by sonication. The GST-fusion protein was purified over glutathione Agarose resin (Fisher), and the GST tag was cleaved

with Prescission protease. The protein was concentrated into 20 mM Tris pH 6.8, in the presence of 150 mM NaCl and 3 mM DTT. ^{1}H,^{15}N heteronuclear single quantum coherence (HSQC) spectra were recorded on a 0.1 mM PHD$_{1-2}$ sample on a 600 MHz Varian INOVA spectrometer in the presence of increasing concentrations of a histone H3 tail peptide (1-12) (synthesized by the UCD Biophysics Core Facility).

Surface plasmon resononance

All measurements were made with the isolated PHD-finger domains cleaved of the GST-affinity tag on a BIAcore 2000 instrument. Biotinylated histone H3 peptides (1-11) were immobilized onto the SA sensor chip by flowing 5 μL of 2 μg/mL H3 peptide solution in HBST buffer (10 mM Hepes; 150 mM NaCl; 0.005% NP-4 0; pH 7.5). Data were acquired by passing increasing concentrations (0-100 μM) of CHD5 PHD-finger over the sensor chip for 2 min at a flow rate of 30 μL/min. The sensor chip surface was regenerated by flowing a strip solution (1 M NaCl) for 5s at a flow rate of 30 μL/min. The dissociation constants (K_d) were obtained by fitting the data with BIAevaulation software to a 1:1 Langmuir and bivalent binding model (PHD$_{1-2}$).

Results

CHD5 PHD$_1$ and PHD$_2$ recognize the N-terminus of histone H3

To investigate the binding specificity of the individual PHD-fingers from chromodomain, helicase DNA-binding protein 5 (CHD5), two distinct platforms of histone post-translational peptide libraries were employed. One platform involves a targeted, spatially-addressed library of 16 different PTM states from histone H3 and H4, while the second platform contains a 5000-member combinatorial histone H3 library on beads (46).

The miniature 16-member histone peptide library was devised around relevant post-translational modifications (PTMs) on histone H3 and H4 (Figure 2a) using celluspot peptide synthesis (47). After parallel peptide synthesis, the library was microarrayed on white-foil coated microscope slides (Intavis). Each peptide was arrayed 16 times to account for irregularities on the slide surface. A single library fits onto a 2 cm × 2 cm square space on the slide surface and contains a total of 256 peptide spots. Glutathione S-transferase (GST)-tagged versions of the PHD-fingers were recombinantly expressed and purified. To interrogate the binding specificity of the CHD5 PHD-fingers (Figure 2b), the GST-fusion proteins were incubated with the library and the ability to bind the peptide arrays was assessed using an anti-GST biotinylated antibody. After appropriate wash steps, addition of streptavidin-conjugated Alexa Fluor 647 permitted the quantification of binding as the intensity of fluorescence emission at 647 nm. Fluorescence intensity at each 16-replicate spots was averaged and the standard deviation calculated. The values were then normalized to the highest intensity spot in the screen.

Binding analysis revealed that both PHD$_1$ and PHD$_2$ specifically bind to unmodified forms of the histone H3 N-terminus. The CHD5-PHD$_1$ displayed significantly lower overall signal intensity compared to CHD5-PHD$_2$ (Figure 2c-d). Separately, each domain displayed highest preference for the completely unmodified form of the first 11 amino acids of the H3 N-terminus (peptide #2). Compared with unmodified H3, there was a slight reduction in signal intensity when arginine-2 contains symmetric dimethylation (peptide #15) and a major decrease (>90%) in signal when lysine-4 is trimethylated (peptide #1). Interestingly, there was no detectable binding signal when threonine 3 is phosphorylated (peptide #11). The lack of binding to other H3 and H4 sequences, and the observation that no signal was detected for the H3 peptide containing amino acids 4-14 (peptide # 4) yielded sequence specific binding information for both PHD$_1$ and PHD$_2$ (Figure 2c-d). Peptide #4 lacked the

three most N-terminal amino acids (ART) on H3, indicating the importance of these three residues for binding affinity.

To corroborate and expand on the results from the microarray peptide library, a 5,000-member combinatorial H3 library was employed. This H3 one-bead one-peptide library was previously used to explore the binding specificity of other chromatin reader domains (46). Briefly, the library was incubated first with the glutathione S-transferase (GST)-tagged versions of the PHD-fingers, second with a GST-specific primary antibody, third with a biotinylated secondary antibody and finally with streptavidin-conjugated alkaline phosphatase (SAAP). Addition and hydrolysis of the SAAP substrate 5-bromo-4-chloro-3-indolyl phosphate (BCIP) resulted in formation of a turquoise precipitate on beads bearing sequences that bound to the target protein. Color development was allowed to proceed for ~15 minutes. Eleven dark blue beads were chosen for PHD_1 analysis and for PHD_2 fifty-five dark blue beads were chosen (Full sequences can be found in Supplementary Tables 1-2). The fewer observed positive beads in the PHD_1 screen suggested weaker overall affinity for H3 compared with PHD_2. The peptides from individual beads in both screens were cleaved and the PTM patterns were identified by MALDI-TOF analysis (Figure 2e-f), as previously described (46).

To assess which PTM states affected overall binding efficiency, discrimination factors were calculated by taking the frequency of that particular PTM among the blue beads (positive hits) divided by the frequency of that PTM observed in a random pool of 100 beads. The magnitude of the discrimination factor correlates with binding preferences at each variable position and corrects for any synthetic bias in library construction (Figure 2e-f). Black bars at the various amino acid positions represent modifications states that were particularly important for the binding interaction while gray bars represent modifications of less importance. The ability to select 55 beads for CHD5-PHD_2 also allowed for a statistically significant chi-squared ($\chi 2$) analysis to determine whether the modification state of a particular position was important for binding (Figure 2f). Chi-squared analysis was not performed on PHD_1 due to lack of sufficient positive hits from the library screen.

Both PHD_1 and PHD_2 displayed strong preference for binding the unmodified form of lysine-4 (9 out of 11 beads for PHD_1; 41 out of 55 for PHD_2) as was denoted by significant discrimination factors in both cases (PHD_1 = 3.9 and PHD_2 = 3.6) (Figure 2e-f). Discrimination against di- and trimethylation is evidenced by the complete lack of either modification in the either screen. The unmodified or monomethylated form of arginine-2 was favored for binding as there was a low occurrence of dimethylation (symmetric and asymmetric) in both PHD-finger screens (0 out of 11 beads for PHD_1; 13 out of 55 for PHD_2). This observation corroborates with the binding data from the miniature microarray library. Both PHD-fingers showed intolerance for phosphorylation of H3T3 (zero occurrences) and H3T6 (0 out of 11 beads for PHD_1; 1 out of 55 for PHD_2). Phosphorylation of H3S10 was also detrimental for binding to both PHD-fingers, demonstrated by the extremely low occurrence of this modification (0 of 11 beads for PHD_1; 9 of 55 for PHD_2).

Taken together, the results from the two screening methods demonstrate the ability of both CHD5 PHD_1 and PHD_2 to recognize the unmodified form of the histone H3 N-terminus. Both PHD-fingers are sensitive to several modifications within the N-terminal region including methylation at both H3R2 and H3K4, and phosphorylation at H3T3, H3T6 and H3S10. Interestingly, modification of either H3R8 or H3K9 did not significantly affect binding. Lastly, the three most N-terminal amino acids (ART) are essential for high affinity binding to each PHD-finger.

The CHD5- PHD$_{1-2}$ tandem domain recognizes the N-terminus of H3 with unaltered specificity

To evaluate whether the tandem linked domain of PHD$_{1-2}$ displays equivalent binding specificity when compared with the individual PHD-fingers, the tandem domain was screened using the miniature spatially-addressed histone library and a 5,000-member combinatorial histone H3 library. Binding analysis from the spatially addressed library screen revealed a nearly identical profile for PHD$_{1-2}$ compared with PHD$_1$ and PHD$_2$ alone (Figure 3a). The linked PHD fingers PHD$_{1-2}$ are specific for the unmodified form of the histone H3 N-terminus (peptide #2). There is a slight reduction in signal intensity when arginine-2 contains symmetric dimethylation (peptide #15) and about 75% signal reduction when lysine-4 is trimethylated (peptide #1). There was no detectable signal above background when threonine 3 is phosphorylated (peptide #11). The observation that no signal was present for peptide # 4 again demonstrated the importance of the three most N-terminal amino acids (ART) (Figure 3a).

Next, the tandem PHD$_{1-2}$ was screened against the 5,000-member combinatorial histone H3 library. A high occurrence of positive hits (90 selected) allowed for positional chi-squared analysis (Figure 3b; Supplementary Table 3). As with the screens for PHD$_1$ and PHD$_2$, discrimination factors were calculated by taking the frequency of a particular PTM among the blue beads (positive hits) and dividing by the frequency of that PTM observed in a random pool of 100 beads. Similar to the results with the individual PHD-finger screens, there was a strong preference for the unmodified form of H3K4 (discrimination factor of 2.3; 44 out of 90 beads) (Figure 3b). There was a high degree of discrimination against phosphorylation at H3T3 (0 out of 90 beads) and H3T6 (0 out of 90 beads), consistent with the trends observed for the individual PHD-fingers. Phosphorylation of H3S10 was also a statistically significant modification by chi-squared analysis, though less of a negative influence on binding compared with either H3T3 or H3T6, as noted by a higher occurrence of H3S10ph in the screen (24 out of 66 beads).

The greater number of positive hits in the PHD$_{1-2}$ screen suggested tighter overall binding relative to the two domains individually. This allowed us to include additional hits that displayed slightly weaker binding (lighter shades of blue). Inclusion of these data permitted an interesting "methylation cross talk" analysis to be performed (Figure 3c; Supplementary Tables 4-5). There was a higher occurrence of dimethylation (both symmetric and asymmetric) at H3R2 and di/trimethylation at H3K4 when compared with PHD$_1$ or PHD$_2$ alone. About 39% of peptides from the screen contain either Rme2a or Rme2s. The occurrence of these modifications decreases to 17% when analyzing peptides that also contain high methylation at H3K4 (me2/3) demonstrating sensitivity of PHD$_{1-2}$ to the overall methylation state of the peptide. Similarly, the occurrence of peptides containing low methylation at H3R2 (R2unmod or R2me1) increases from 56% (in all peptides) to 86% (peptides containing only Kme2/3 at H3K4).

The occurrence of peptides containing high methylation at H3K4 (me2/3) decreases from 13% to 6% when analyzing peptides that also contain R2me2a or R2me2s (Figure 3c). Similarly, occurrence of peptides with low methylation at H3K4 (K4unmod and K4me) increases from 74% (in all peptides) to 91% (peptides only containing Rme2a/s at H3R2). This understates the deleterious effect methylation of the N-terminus at these two positions has for PHD$_{1-2}$ recognition and demonstrates a combinatorial negative binding effect when the overall methylation state of the H3 N-terminus is high.

Although the binding profile for the tandem domain was similar to that of PHD$_1$ and PHD$_2$, the overall signal intensity for PHD$_{1-2}$ was notably higher in both peptide screens compared to either domain alone (at the same molar concentrations). This implied a stronger

interaction between PHD_{1-2} and the H3 N-terminus that had two plausible general mechanistic explanations: 1. Both domains concomitantly engage a single copy of the H3 N-terminus resulting in an overall higher affinity or 2. Each PHD domain binds a distinct copy of the H3 N-terminus resulting in a higher binding affinity (avidity) due to bivalent engagement.

The tandem CHD5-PHD$_{1-2}$ engages two copies of the H3 N-terminus

After demonstrating that both individual PHD-fingers from CHD5 recognize the unmodified N-terminus of histone H3, and that the two together do not have altered specificity, the binding mechanism was further explored using several techniques. To explore the likelihood that PHD_{1-2} can bind two distinct copies of the H3 N-terminus, an Amplified Luminescent Proximity Homogeneous Assay (ALPHA) was employed (Figure 4a). Signal from the ALPHA depends on the proximity of a streptavidin-functionalized donor bead and Ni^{2+}-chelated acceptor bead. Donor beads contain a photosensitizer, phthalocyanine, which converts ambient oxygen to an excited form of singlet oxygen upon illumination at 680 nm. Within its 4-μsec half-life, the singlet oxygen can diffuse approximately 200 nm in solution. If an acceptor bead is within that proximity, energy is transferred from the singlet oxygen to thioxene derivatives within the acceptor bead, culminating in light production at 520–620 nm. In the absence of an acceptor bead, the singlet oxygen falls to ground state and no signal is produced.

Two identical peptides pertaining to the first eleven amino acids of the H3 N-terminus were functionalized with either biotin or 6×-histidine at their C-terminus to facilitate interaction with the ALPHA donor and acceptor beads respectively. The proximity of these differentially functionalized peptides in the presence of CHD5-PHD$_{1-2}$ resulted in a significant increase in florescent signal intensity when compared with the CHD5-PHD$_1$ (96% increase) or CHD5-PHD$_2$ (82% increase) single domains (Figure 4b). There was no signal above background when PHD$_{1-2}$ was incubated with either functionalized peptide alone or when both peptides were incubated in the absence of protein. For comparison, we analyzed the single PHD-finger from BHC80, which also binds H3K4unmod (42, 46). BHC80 showed 95% lower signal intensity when compared with CHD5-PHD$_{1-2}$, consistent with the inability of BHC80 to bind simultaneously two peptides. These results suggest the unique capability of PHD$_{1-2}$ to engage two individual copies of the unmodified histone H3 N-terminus.

To corroborate the results of the ALPHA, NMR titrations were employed. $^1H,^{15}N$ HSQC spectra of uniformly ^{15}N-labeled PHD$_{1-2}$ were collected while titrating in a peptide corresponding to the 12 most N-terminal residues of histone H3. Addition of increasing amounts of the peptide induced substantial chemical shift changes in the PHD$_{1-2}$ spectrum. The pattern of resonance perturbations indicated that there are two distinct binding events in PHD$_{1-2}$, with the resonances of PHD$_2$ shifting significantly upon the first addition of peptide. The CHD5-PHD$_2$ begins to saturate at a ~1:2 protein: peptide molar ratio (yellow), while saturation of PHD$_1$ only starts at ~1:10 (blue) (Figure 5). Together this data suggests that each PHD domain binds a distinct histone H3 tail peptide and that PHD$_2$ has a slightly higher affinity for the H3 peptide than does PHD$_1$.

To demonstrate that bivalent association explains the increased apparent affinity of PHD$_{1-2}$ for immobilized H3 N-terminal peptides, a modified version of the celluspot library was employed (Figure 6a). In this "dilution libraryp" a single peptide encompassing the first 11 amino acids of histone H3 was synthesized using the celluspot technique (47). The stock solution of H3 peptide was diluted to yield eight concentrations over two orders of magnitude and subsequently arrayed in duplicate on a slide surface (Figure 6a). The GST-based detection assay (Figure 2b) was used to compare relative affinities of the linked

tandem PHD_{1-2} domain against single PHD_2 or the combination of unlinked $PHD_2 + PHD_1$. The signal from four replicate dilution libraries was averaged (8 replicates per peptide concentration) and the standard deviation calculated (Figure 6b-c).

The interaction of the linked PHD_{1-2} with H3 N-termini of the dilution library yielded fluorescent signals that were ~10 times higher than PHD_2 alone (Figure 6c). The signal from PHD_1 at this concentration was too low to quantify accurately (data not shown). To illustrate that the 10-fold signal increase for linked PHD_{1-2} is not based solely on the presence of both domains in the assay, a combination of unlinked $PHD_1 + PHD_2$ was tested. The unlinked combination showed only a slight increase in signal intensity compared to PHD_2 alone (Figure 6c). These data underscore the importance of connecting the two domains together to achieve overall higher affinity from an avidity effect.

Next, we utilized surface plasmon resonance and immobilized histone H3 (1-11) to assess whether the apparent increase in affinity of the tandem PHD_{1-2} is due to avidity, which would be reflected in the dissociation. Response curves were acquired by passing increasing concentrations (0-100 μM) of CHD5 PHD-finger constructs over the sensor chip containing immobilized histone H3. Curves were fitted with BIAevaluation software and the results are summarized in Table 1. Sensorgram data from PHD_{1-2}, PHD_1 and PHD_2 were fitted to a 1:1 langmuir model, and additionally to a bivalent binding model for PHD_{1-2} (Supplementary Figures 1-3). From the 1:1 langmuir model, the estimated K_d value for PHD_{1-2}, was 4-11 lower than PHD_1 and PHD_2 alone. Importantly, the a bivalent binding model for the PHD_{1-2} sensorgrams yielded a much better fit. Consistent with the apparent K_d difference in the 1:1 langmuir fits, the last off-rate (k_d) for PHD_{1-2} is 5-6 fold slower than the k_d values derived from the individual domains (Table 1). The magnitude change in affinity (difference in dissociation) measured from the dilution library and SPR experiments is similar to results obtained from bivalent antibodies compared with their monovalent Fab fragments (48). Together with the NMR titrations, the dilution peptide library, and the ALPHA, these results demonstrate the ability of CHD5-PHD_{1-2} to recognize two distinct copies of the unmodified H3 N-terminus, leading to an important avidity effect that provides direct evidence for the binding capacity of tandem reader domains.

Discussion

The ability of linked chromatin binding modules to independently recognize different regions of histones is generally believed to be a critical component of protein complexes that must interpret the diversity in the histone PTM language. However, there is relatively little biochemical evidence to support this hypothesis. There are a few reports where tandem PHD-Bromo domains specifically recognize histone modifications in cis, i.e. on the same histone protein (H3K4unmod and H3K23ac) or in trans, i.e. on different histone proteins (H3K4me3 and H4K16ac) (40, 41, 49). In these studies, the ability of tandem PHD-bromo domains to independently recognize dual modification states plays two central roles. The first is the enhanced specificity that dual recognition confers for these proteins. It allows the proteins to target very specific regions of chromatin where both modification states co-exist. The second is the enhanced strength of interaction that is provided by contacting two histone regions. Dissociation of polyvalent chromatin interactions requires breaking *n* modification + *n* module interactions; it is therefore predicted that dissociation occurs more slowly in the polyvalent interaction than in corresponding monovalent interactions. This is essentially an avidity effect where transient unbinding of a single module does not allow the protein to diffuse away, and rebinding of that module is more probable, leading to an overall enhancement in affinity.

The results presented in this study suggest that the tandem PHD fingers of CHD5 employ bivalent ligand recognition of unmodified histone H3 N-termini to recruit/stabilize CHD5-containing complexes at targeted genomic loci. Intriguingly, it appears that CHD5 activity is required for appropriate transcription of the *Ink4/Arf* gene locus (27, 29), which is an upstream activator of the tumor suppressor p53. We hypothesize that the bivalent interaction of the tandem PHD-fingers may facilitate transcription at such loci through recruitment or stabilization of CHD5. Because of the densely packed heterochromatic structure at this normally repressed region there is likely a high density of unmodified (at H3K4) histone tails. The existence of regions of chromatin where the unmodified N-terminus of H3 is dense would serve as an excellent recognition platform for the tandem PHD-fingers. Consistent with our findings, the presence of H3K9me3 (a modification highly associated with compact heterochromatin) would not affect the ability of CHD5-PHD$_{1-2}$ to recognize histone H3. Previous studies with the closely related CHD4 PHD-fingers report a slight enhancement of binding in the presence of this modification (45, 50, 51). Overall, our studies elucidate the mechanistic basis for initial observations that binding of the NuRD complex was inhibited by H3K4 methylation (52)(53).

CHD5-PHD$_{1-2}$ recognition of histone H3 might serve as an initial step in an ATPase dependent chromatin-remodeling transition from repressed to transcriptionally active chromatin. This is an intriguing possibility considering a recent study that demonstrates the necessity of the dual CHD4 PHD-fingers for maintaining the *repressive* function of the CHD4/NuRD complex (45). Musselman et al proposed that the CHD4 PHD-fingers can recognize histone H3 tails on the same nucleosome, but the possibility of internucleosomal recognition for the CHD4 or CHD5 PHD-fingers cannot be ruled out. There is significant evidence that the NuRD complex can function either in gene activation or gene repression in different contexts, though a mechanistic understanding is still unknown (11, 54). It is appealing to speculate that interexchange of CHD4 and CHD5 within the NuRD complex may drive the specificity, and thus the decision of the resulting complex to act as either a repressor or activator of transcription, respectively. Nevertheless, these biochemical studies provide the framework for understanding how multiple chromatin binding modules function to interpret the combinatorial PTM capacity written in chromatin.

Supplementary Material

Refer to Web version on PubMed Central for supplementary material.

Acknowledgments

References

1. Marfella CG, Imbalzano AN. The Chd family of chromatin remodelers. Mutat Res. 2007; 618:30–40. [PubMed: 17350655]

2. Li DQ, Kumar R. Mi-2/NuRD complex making inroads into DNA-damage response pathway. Cell Cycle. 2010; 9:2071–2079. [PubMed: 20505336]

3. Ramirez J, Hagman J. The Mi-2/NuRD complex: a critical epigenetic regulator of hematopoietic development, differentiation and cancer. Epigenetics. 2009; 4:532–536. [PubMed: 19923891]

4. Denslow SA, Wade PA. The human Mi-2/NuRD complex and gene regulation. Oncogene. 2007; 26:5433–5438. [PubMed: 17694084]

5. Bowen NJ, Fujita N, Kajita M, Wade PA. Mi-2/NuRD: multiple complexes for many purposes. Biochim Biophys Acta. 2004; 1677:52–57. [PubMed: 15020045]

6. Lai AY, Wade PA. Cancer biology and NuRD: a multifaceted chromatin remodelling complex. Nat Rev Cancer. 2011; 11:588–596. [PubMed: 21734722]

7. Reynolds N, Salmon-Divon M, Dvinge H, Hynes-Allen A, Balasooriya G, Leaford D, Behrens A, Bertone P, Hendrich B. NuRD-mediated deacetylation of H3K27 facilitates recruitment of Polycomb Repressive Complex 2 to direct gene repression. Embo J. 2011; 31:593–605. [PubMed: 22139358]

8. Zhang Y. Biology of the Mi-2/NuRD Complex in SLAC (Stemness, Longevity/Ageing, and Cancer). Gene Regul Syst Bio. 2011; 5:1–26.

9. Sims JK, Wade PA. Mi-2/NuRD complex function is required for normal S phase progression and assembly of pericentric heterochromatin. Mol Biol Cell. 2011; 22:3094–3102. [PubMed: 21737684]

10. Hung H, Kohnken R, Svaren J. The nucleosome remodeling and deacetylase chromatin remodeling (NuRD) complex is required for peripheral nerve myelination. J Neurosci. 2012; 32:1517–1527. [PubMed: 22302795]

11. Williams CJ, Naito T, Arco PG, Seavitt JR, Cashman SM, De Souza B, Qi X, Keables P, Von Andrian UH, Georgopoulos K. The chromatin remodeler Mi-2beta is required for CD4 expression and T cell development. Immunity. 2004; 20:719–733. [PubMed: 15189737]

12. Thompson PM, Gotoh T, Kok M, White PS, Brodeur GM. CHD5, a new member of the chromodomain gene family, is preferentially expressed in the nervous system. Oncogene. 2003; 22:1002–1011. [PubMed: 12592387]

13. Potts RC, Zhang P, Wurster AL, Precht P, Mughal MR, Wood WH 3rd, Zhang Y, Becker KG, Mattson MP, Pazin MJ. CHD5, a brain-specific paralog of Mi2 chromatin remodeling enzymes, regulates expression of neuronal genes. PLoS One. 2011; 6:e24515. [PubMed: 21931736]

14. Wang X, Lau KK, So LK, Lam YW. CHD5 is down-regulated through promoter hypermethylation in gastric cancer. J Biomed Sci. 2009; 16:95. [PubMed: 19840376]

15. Zhao R, Yan Q, Lv J, Huang H, Zheng W, Zhang B, Ma W. CHD5, a tumor suppressor that is epigenetically silenced in lung cancer. Lung Cancer. 2012; 76:324–331. [PubMed: 22186629]

16. Wang J, Chen H, Fu S, Xu ZM, Sun KL, Fu WN. The involvement of CHD5 hypermethylation in laryngeal squamous cell carcinoma. Oral Oncol. 2011; 47:601–608. [PubMed: 21636313]

17. Cai C, Ashktorab H, Pang X, Zhao Y, Sha W, Liu Y, Gu X. MicroRNA-211 expression promotes colorectal cancer cell growth in vitro and in vivo by targeting tumor suppressor CHD5. PLoS One. 2012; 7:e29750. [PubMed: 22235338]

18. Mulero-Navarro S, Esteller M. Chromatin remodeling factor CHD5 is silenced by promoter CpG island hypermethylation in human cancer. Epigenetics. 2008; 3:210–215. [PubMed: 18698156]

19. Gorringe KL, Choong DY, Williams LH, Ramakrishna M, Sridhar A, Qiu W, Bearfoot JL, Campbell IG. Mutation and methylation analysis of the chromodomain-helicase-DNA binding 5 gene in ovarian cancer. Neoplasia. 2008; 10:1253–1258. [PubMed: 18953434]

20. Lang J, Tobias ES, Mackie R. Preliminary evidence for involvement of the tumour suppressor gene CHD5 in a family with cutaneous melanoma. Br J Dermatol. 2011; 164:1010–1016. [PubMed: 21250965]

21. Law ME, Templeton KL, Kitange G, Smith J, Misra A, Feuerstein BG, Jenkins RB. Molecular cytogenetic analysis of chromosomes 1 and 19 in glioma cell lines. Cancer Genet Cytogenet. 2005; 160:1–14. [PubMed: 15949564]

22. Mokarram P, Kumar K, Brim H, Naghibalhossaini F, Saberi-firoozi M, Nouraie M, Green R, Lee E, Smoot DT, Ashktorab H. Distinct high-profile methylated genes in colorectal cancer. PLoS One. 2009; 4:e7012. [PubMed: 19750230]

23. Okawa ER, Gotoh T, Manne J, Igarashi J, Fujita T, Silverman KA, Xhao H, Mosse YP, White PS, Brodeur GM. Expression and sequence analysis of candidates for the 1p36.31 tumor suppressor gene deleted in neuroblastomas. Oncogene. 2008; 27:803–810. [PubMed: 17667943]

24. Robbins CM, Tembe WA, Baker A, Sinari S, Moses TY, Beckstrom-Sternberg S, Beckstrom-Sternberg J, Barrett M, Long J, Chinnaiyan A, Lowey J, Suh E, Pearson JV, Craig DW, Agus DB,

Pienta KJ, Carpten JD. Copy number and targeted mutational analysis reveals novel somatic events in metastatic prostate tumors. Genome Res. 2011; 21:47–55. [PubMed: 21147910]

25. Wong RR, Chan LK, Tsang TP, Lee CW, Cheung TH, Yim SF, Siu NS, Lee SN, Yu MY, Chim SS, Wong YF, Chung TK. CHD5 Downregulation Associated with Poor Prognosis in Epithelial Ovarian Cancer. Gynecol Obstet Invest. 2011; 72:203–207. [PubMed: 21860208]

26. Garcia I, Mayol G, Rodriguez E, Sunol M, Gershon TR, Rios J, Cheung NK, Kieran MW, George RE, Perez-Atayde AR, Casala C, Galvan P, de Torres C, Mora J, Lavarino C. Expression of the neuron-specific protein CHD5 is an independent marker of outcome in neuroblastoma. Mol Cancer. 2010; 9:277. [PubMed: 20950435]

27. Bagchi A, Papazoglu C, Wu Y, Capurso D, Brodt M, Francis D, Bredel M, Vogel H, Mills AA. CHD5 is a tumor suppressor at human 1p36. Cell. 2007; 128:459–475. [PubMed: 17289567]

28. Fujita T, Igarashi J, Okawa ER, Gotoh T, Manne J, Kolla V, Kim J, Zhao H, Pawel BR, London WB, Maris JM, White PS, Brodeur GM. CHD5, a tumor suppressor gene deleted from 1p36.31 in neuroblastomas. J Natl Cancer Inst. 2008; 100:940–949. [PubMed: 18577749]

29. Bagchi A, Mills AA. The quest for the 1p36 tumor suppressor. Cancer Res. 2008; 68:2551–2556. [PubMed: 18413720]

30. Musselman CA, Kutateladze TG. Handpicking epigenetic marks with PHD fingers. Nucleic Acids Res. 2011; 39:9061–9071. [PubMed: 21813457]

31. Musselman CA, Kutateladze TG. PHD fingers: epigenetic effectors and potential drug targets. Mol Interv. 2009; 9:314–323. [PubMed: 20048137]

32. Sanchez R, Zhou MM. The PHD finger: a versatile epigenome reader. Trends Biochem Sci. 2011; 36:364–372. [PubMed: 21514168]

33. Kwan AH, Gell DA, Verger A, Crossley M, Matthews JM, Mackay JP. Engineering a protein scaffold from a PHD finger. Structure. 2003; 11:803–813. [PubMed: 12842043]

34. Li H, Ilin S, Wang W, Duncan EM, Wysocka J, Allis CD, Patel DJ. Molecular basis for site-specific read-out of histone H3K4me3 by the BPTF PHD finger of NURF. Nature. 2006; 442:91–95. [PubMed: 16728978]

35. Pena PV, Davrazou F, Shi X, Walter KL, Verkhusha VV, Gozani O, Zhao R, Kutateladze TG. Molecular mechanism of histone H3K4me3 recognition by plant homeodomain of ING2. Nature. 2006; 442:100–103. [PubMed: 16728977]

36. Zhang Y. It takes a PHD to interpret histone methylation. Nat Struct Mol Biol. 2006; 13:572–574. [PubMed: 16826231]

37. Mellor J. It takes a PHD to read the histone code. Cell. 2006; 126:22–24. [PubMed: 16839870]

38. Taverna SD, Li H, Ruthenburg AJ, Allis CD, Patel DJ. How chromatin-binding modules interpret histone modifications: lessons from professional pocket pickers. Nat Struct Mol Biol. 2007; 14:1025–1040. [PubMed: 17984965]

39. Taverna SD, Ilin S, Rogers RS, Tanny JC, Lavender H, Li H, Baker L, Boyle J, Blair LP, Chait BT, Patel DJ, Aitchison JD, Tackett AJ, Allis CD. Yng1 PHD finger binding to H3 trimethylated at K4 promotes NuA3 HAT activity at K14 of H3 and transcription at a subset of targeted ORFs. Mol Cell. 2006; 24:785–796. [PubMed: 17157260]

40. Ruthenburg AJ, Li H, Milne TA, Dewell S, McGinty RK, Yuen M, Ueberheide B, Dou Y, Muir TW, Patel DJ, Allis CD. Recognition of a mononucleosomal histone modification pattern by BPTF via multivalent interactions. Cell. 2011; 145:692–706. [PubMed: 21596426]

41. Zeng L, Zhang Q, Li S, Plotnikov AN, Walsh MJ, Zhou MM. Mechanism and regulation of acetylated histone binding by the tandem PHD finger of DPF3b. Nature. 2010; 466:258–262. [PubMed: 20613843]

42. Lan F, Collins RE, De Cegli R, Alpatov R, Horton JR, Shi X, Gozani O, Cheng X, Shi Y. Recognition of unmethylated histone H3 lysine 4 links BHC80 to LSD1-mediated gene repression. Nature. 2007; 448:718–722. [PubMed: 17687328]

43. Koh AS, Kuo AJ, Park SY, Cheung P, Abramson J, Bua D, Carney D, Shoelson SE, Gozani O, Kingston RE, Benoist C, Mathis D. Aire employs a histone-binding module to mediate immunological tolerance, linking chromatin regulation with organ-specific autoimmunity. Proc Natl Acad Sci U S A. 2008; 105:15878–15883. [PubMed: 18840680]

44. Wang Z, Patel DJ. Combinatorial readout of dual histone modifications by paired chromatin-associated modules. J Biol Chem. 2011; 286(21):18363–18368. [PubMed: 21454653]

45. Musselman CA, Ramirez J, Sims JK, Mansfield RE, Oliver SS, Denu JM, Mackay JP, Wade PA, Hagman J, Kutateladze TG. Bivalent recognition of nucleosomes by the tandem PHD fingers of the CHD4 ATPase is required for CHD4-mediated repression. Proc Natl Acad Sci U S A. 2012; 109:787–792. [PubMed: 22215588]

46. Garske AL, Oliver SS, Wagner EK, Musselman CA, LeRoy G, Garcia BA, Kutateladze TG, Denu JM. Combinatorial profiling of chromatin binding modules reveals multisite discrimination. Nat Chem Biol. 2010; 6:283–290. [PubMed: 20190764]

47. Winkler DF, Hilpert K, Brandt O, Hancock RE. Synthesis of peptide arrays using SPOT-technology and the CelluSpots-method. Methods in molecular biology Clifton, N.J. 2009; 570:157–174.

48. Mack ET, Snyder PW, Perez-Castillejos R, Whitesides GM. Using covalent dimers of human carbonic anhydrase II to model bivalency in immunoglobulins. J Am Chem Soc. 2011; 133:11701–11715. [PubMed: 21671600]

49. Tsai WW, Wang Z, Yiu TT, Akdemir KC, Xia W, Winter S, Tsai CY, Shi X, Schwarzer D, Plunkett W, Aronow B, Gozani O, Fischle W, Hung MC, Patel DJ, Barton MC. TRIM24 links a non- canonical histone signature to breast cancer. Nature. 2010; 468:927–932. [PubMed: 21164480]

50. Mansfield RE, Musselman CA, Kwan AH, Oliver SS, Garske AL, Davrazou F, Denu JM, Kutateladze TG, Mackay JP. Plant Homeodomain (PHD) Fingers of CHD4 Are Histone H3-binding Modules with Preference for Unmodified H3K4 and Methylated H3K9. J Biol Chem. 2011; 286:11779–11791. [PubMed: 21278251]

51. Musselman CA, Mansfield RE, Garske AL, Davrazou F, Kwan AH, Oliver SS, O'Leary H, Denu JM, Mackay JP, Kutateladze TG. Binding of the CHD4 PHD2 finger to histone H3 is modulated by covalent modifications. Biochem J. 2009; 423:179–187. [PubMed: 19624289]

52. Zegerman P, Canas B, Pappin D, Kouzarides T. Histone H3 lysine 4 methylation disrupts binding of nucleosome remodeling and deacetylase (NuRD) repressor complex. J Biol Chem. 2002; 277:11621–11624. [PubMed: 11850414]

53. Nishioka K, Chuikov S, Sarma K, Erdjument-Bromage H, Allis CD, Tempst P, Reinberg D. Set9, a novel histone H3 methyltransferase that facilitates transcription by precluding histone tail modifications required for heterochromatin formation. Genes Dev. 2002; 16:479–489. [PubMed: 11850410]

54. Miccio A, Wang Y, Hong W, Gregory GD, Wang H, Yu X, Choi JK, Shelat S, Tong W, Poncz M, Blobel GA. NuRD mediates activating and repressive functions of GATA-1 and FOG-1 during blood development. Embo J. 2010; 29:442–456. [PubMed: 19927129]

55. Berger MF, Lawrence MS, Demichelis F, Drier Y, Cibulskis K, Sivachenko AY, Sboner A, Esgueva R, Pflueger D, Sougnez C, Onofrio R, Carter SL, Park K, Habegger L, Ambrogio L, Fennell T, Parkin M, Saksena G, Voet D, Ramos AH, Pugh TJ, Wilkinson J, Fisher S, Winckler W, Mahan S, Ardlie K, Baldwin J, Simons JW, Kitabayashi N, MacDonald TY, Kantoff PW, Chin L, Gabriel SB, Gerstein MB, Golub TR, Meyerson M, Tewari A, Lander ES, Getz G, Rubin MA, Garraway LA. The genomic complexity of primary human prostate cancer. Nature. 2011; 470:214–220. [PubMed: 21307934]
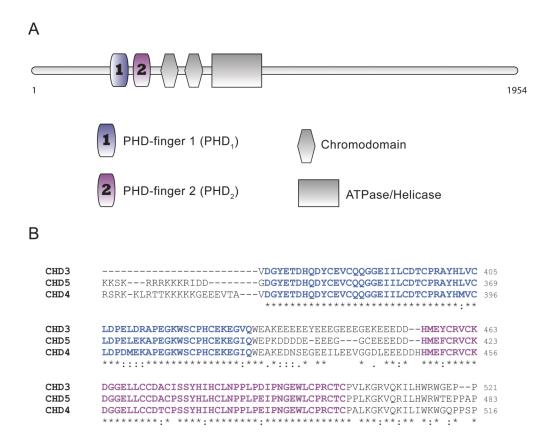
A


```
1  PHD-finger 1 (PHD₁)          Chromodomain

2  PHD-finger 2 (PHD₂)          ATPase/Helicase
```

B

```
CHD3    ------------------------VDGYETDHQDYCEVCQQGGEIILCDTCPRAYHLVC 405
CHD5    KKSK---RRRKKKKRIDD--------GDGYETDHQDYCEVCQQGGEIILCDTCPRAYHLVC 369
CHD4    RSRK-KLRTTKKKKKGEEEVTA---VDGYETDHQDYCEVCQQGGEIILCDTCPRAYHMVC 396
                                **************************** :**

CHD3    LDPELDRAPEGKWSCPHCEKEGVQWEAKEEEEEYEEEGEEEGEKEEEDD--HMEYCRVCK 463
CHD5    LDPELEKAPEGKWSCPHCEKEGIQWEPKDDDDE-EEEG---GCEEEEDD--HMEFCRVCK 423
CHD4    LDPDMEKAPEGKWSCPHCEKEGIQWEAKEDNSEGEEILEEVGGDLEEEDDHHMEFCRVCK 456
        ***::::*****************:***.*:::.* **     * . **:*  ***:*****

CHD3    DGGELLCCDACISSYHIHCLNPPLPDIPNGEWLCPRCTCPVLKGRVQKILHWRWGEP--P 521
CHD5    DGGELLCCDACPSSYHLHCLNPPLPEIPNGEWLCPRCTCPPLKGKVQRILHWRWTEPPAP 483
CHD4    DGGELLCCDTCPSSYHIHCLNPPLPEIPNGEWLCPRCTCPALKGKVQKILIWKWGQPPSP 516
        *********:* ****:********:************** ***:**:** *:* :*  *
```

Figure 1. CHD3-5 protein architecture and sequence alignment

(A) A cartoon representation showing the N-terminal domain architecture of the highly similar CHD3-5. (B) A sequence alignment for the tandem PHD-fingers of CHD3-5. The first PHD-finger is highlighted in blue and the second in purple. Asterisks (*) denote invariant residues while colons (:) represent conserved residues.
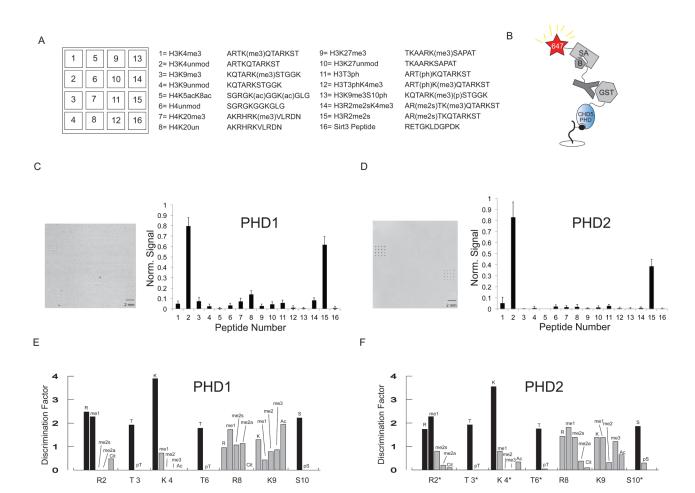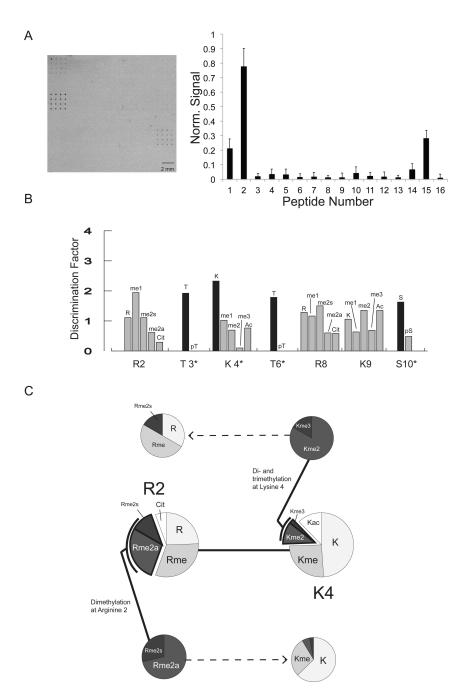
Figure 2. The CHD5-PHD$_1$ and CHD-PHD$_2$ individual domains recognize H3unmod
(A) Each numbered box represents the space in which a single peptide resides (numbered key to the right). Within each numbered box a peptide is arrayed 16 times in a 4×4 spot grid to account for surface and spotting irregularities. (B) The GST-based assay used to determine the binding specificity of the PHD-fingers. B = biotin; SA = streptavidin; 647 = Alexa Fluor-647 (C,D) Raw images for the PHD$_1$ and PHD$_2$ screens (left panels). Values in the bar graphs were obtained by averaging the signal from 16 replicate spots. The values were normalized to the highest intensity spot in each individual library screen. Standard deviation is represented with error bars. (E,F) Discrimination factors for PHD$_1$ (E) and PHD$_2$ (F). Chi-squared values for each residue were calculated. Serine and threonine residues allow for 1 degree of freedom (DF), whereas lysine and arginine allow for 4 degrees of freedom (DF). Chi-squared values above the 99.9% confidence level for statistical significance are denoted with a single asterisk (*) along the x-axis (1 DF = 10.83 and 4 DF = 18.47).
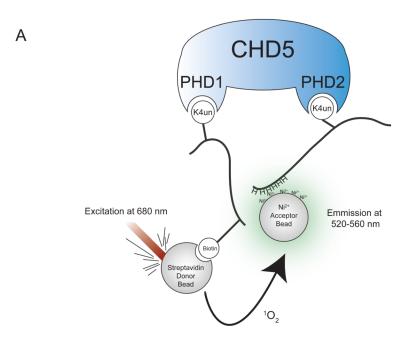
Figure 3. The CHD5-PHD$_{1\text{-}2}$ dual domain recognizes the unmodified histone H3 N- terminus
(A) Values for CHD5-PHD$_{1\text{-}2}$ were obtained by averaging the signal from the 16 replicate peptides arrayed on the slide surface. The values were normalized to the highest intensity spot in each individual library screen and standard deviation was calculated based on variation in signal intensity from the replicate 16 arrayed spots. (B) Discrimination factors for the modification preferences of CHD5-PHD$_{1\text{-}2}$ as previously described (46). (C) The methylation states at H3K4 and H3R2 were analyzed in the context of each other. Peptides containing only Rme2a/s were analyzed to determine their levels of methylation at H3K4 (frequency of methylation states in bottom circle graphs). Peptides containing only Kme2/3

were analyzed to determine the methylation levels at H3R2 (frequency of methylation states denoted in top circle graphs).
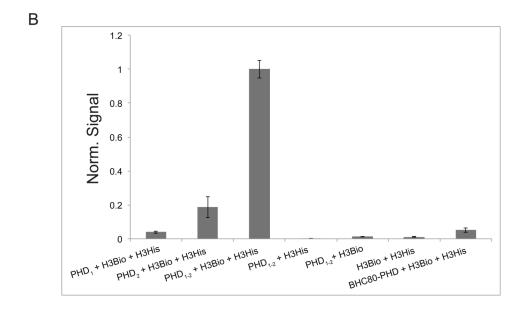
Figure 4. ALPHA assay with CHD5-PHD$_{1-2}$ and H3unmod peptides
(A) Two identical peptides pertaining to the first eleven amino acids of the H3 N-terminus were functionalized with either biotin or 6×-histidine at their C-terminus to facilitate interaction with the ALPHA donor and acceptor beads respectively. Signal from the ALPHA depends on the CHD5-PHD$_{1-2}$ dependent proximity of a streptavidin-functionalized donor bead and Ni^{2+}-chelated acceptor bead. (B) The condition for each ALPHA experiment is labeled along the x-axis. The normalized signal intensity is represented on the y-axis and is the average of three independent experiments. The standard deviation for the three experiments is represented with error bars.
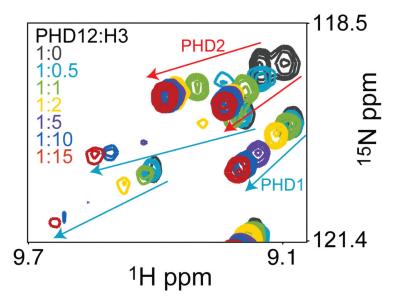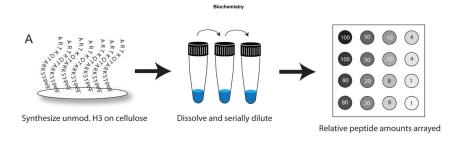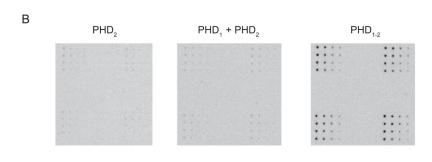
Figure 5. NMR titration of CHD5-PHD$_{1\text{-}2}$ and H3unmod
An overlay of the ^{1}H,^{15}N HSQC spectra of PHD$_{1\text{-}2}$ as increasing amounts of the histone H3 tail peptide (1-12) are titrated in. Spectra are color coded according to the molar ratio of protein: peptide (see inset). Resonances and shifts (denoted by arrows) associated with PHD$_1$ are labeled in blue and those for PHD$_2$ are labeled in red. Overlays of the ^{1}H, ^{15}N HSQC spectra of PHD$_{1\text{-}2}$, PHD$_1$, and PHD$_2$ in the unbound state (Supplementary Figure 4) and bound state (Supplementary Figure 5) are provided in Supplementary data.
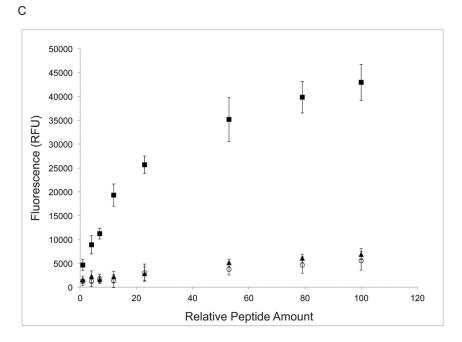
Figure 6. A spatially addressed dilution library with H3unmod peptide
(A) A histone H3 peptide (1-12) was synthesized on modified cellulose discs. The peptide-cellulose conjugate was dissolved in DMSO, diluted over two orders of magnitude, and subsequently arrayed four times in duplicate on a microscope slide surface. (B) The binding ability of CHD5-PHD$_2$ compared with PHD$_1$ + PHD$_2$ and linked PHD$_{1\text{-}2}$ was interrogated with four replicate dilution libraries using a GST-based fluorescent assay. (C) The signal from the four replicate libraries was averaged and plotted against relative cellulose-peptide concentration. Squares represent 0.01 μM PHD$_{1\text{-}2}$ (■), open circles represent 0.01 μM PHD$_2$ (○), and triangles represent 0.01 μM PHD$_1$ + 0.01 μM PHD$_2$ (▲).

Table 1
Kinetic rate constants determined by surface plasmon resonance

The binding on-rate (k_a), off-rate (k_d) and overall dissociation constant (K_d) were determined using a 1:1 Langmuir association model (Table 1; Supplemental figures 1-3). The chi-squared value (Chi^2) denotes the goodness of fit for the binding model. A bivalent analyte binding model was also used to fit the data from PHD_{1-2}.

1:1 Langmuir	k_a (1/Ms)	k_d (1/s)	K_d (M)	Chi^2
PHD_1	104 ± 7	0.0103 ± 0.0001	9.88×10^{-5}	8.94
PHD_2	393 ± 13	0.0136 ± 0.0003	3.46×10^{-5}	0.224
PHD_{1-2}	379 ± 7	$3.48 \times 10^{-3} \pm 5 \times 10^{-5}$	9.18×10^{-6}	27.8

Bivalent binding model	$k_a 1$ (1/Ms)	$k_d 1$ (1/s)	$k_a 2$ (1/RUs)	$k_d 2$ (1/s)	Chi^2
PHD_{1-2}	324 ± 11	0.120 ± 0.005	$2.9 \times 10^{-5} \pm 1 \times 10^{-6}$	$2.18 \times 10^{-3} \pm 3 \times 10^{-5}$	4.82